

Click and Detect: Versatile Ampicillin Aptasensor Enabled by Click Chemistry on a Graphene–Alkyne Derivative

José M. R. Flauzino, Martin-Alex Nalepa, Demetrios D. Chronopoulos, Veronika Šedajová, David Panáček, Petr Jakubec, Petra Kührová, Martin Pykal, Pavel Banáš, Aleš Panáček, Aristides Bakandritsos, and Michal Otyepka*

Tackling the current problem of antimicrobial resistance (AMR) requires fast, inexpensive, and effective methods for controlling and detecting antibiotics in diverse samples at the point of interest. Cost-effective, disposable, point-of-care electrochemical biosensors are a particularly attractive option. However, there is a need for conductive and versatile carbon-based materials and inks that enable effective bioconjugation under mild conditions for the development of robust, sensitive, and selective devices. This work describes a simple and fast methodology to construct an aptasensor based on a novel graphene derivative equipped with alkyne groups prepared via fluorographene chemistry. Using click chemistry, an aptamer is immobilized and used as a successful platform for the selective determination of ampicillin in real samples in the presence of interfering molecules. The electrochemical aptasensor displayed a detection limit of 1.36 nM, high selectivity among other antibiotics, the storage stability of 4 weeks, and is effective in real samples. Additionally, structural and docking simulations of the aptamer shed light on the ampicillin binding mechanism. The versatility of this platform opens up wide possibilities for constructing a new class of aptasensor based on disposable screen-printed carbon electrodes usable in point-of-care devices.

the indiscriminate exposure of microorganisms to antibiotics. This requires controlling antibiotic use and broad monitoring of their levels in complex samples, such as food, tap and wastewater, urine, and blood.^[3] Chromatography and the enzyme-linked immunosorbent assay are considered the gold standard methods for antibiotic detection. However, they are time-consuming and require expensive instrumentation and trained personnel.^[4] Thus, the development of point-of-interest antibiotic detection methods that are fast, cheap, effective, sensitive, and do not require sophisticated laboratory equipment or expert personnel is crucial. To this end, properly designed nano-biosensors meet all the above requirements, combining selective and rapid biorecognition of target analytes with a concentration-dependent signal response for quantitative read-out.^[5]


The most effective biosensors rely on selective recognition of an analyte in a complex sample via specific binding on a high-affinity bioreceptor, which traditionally comprises an enzyme or antibody immobilized on an appropriate support. However, owing to the high cost and difficult handling of such delicate biomolecules, synthetic nucleic acids, such as aptamers, may be better alternatives because they are more stable and simpler to synthesize.^[6] An aptamer's nucleotide sequence can be tailored to selectively bind

1. Introduction

AMR development is becoming one of the most severe threats to public health this century. Worldwide, 4.95 million deaths were associated with AMR in 2019,^[1,2] and the death toll is expected to rise to more than 10 million by 2050.^[2] One of the key measures to restrict the development of AMR is to prevent

J. M. R. Flauzino, M.-A. Nalepa, D. D. Chronopoulos, V. Šedajová, D. Panáček, P. Jakubec, P. Kührová, M. Pykal, P. Banáš, A. Bakandritsos, M. Otyepka
Regional Centre of Advanced Technologies and Materials
Czech Advanced Technology and Research Institute (CATRIN)
Palacký University Olomouc
Šlechtitelů 27, Olomouc 783 71, Czech Republic
E-mail: michal.otyepka@upol.cz

A. Panáček
Department of Physical Chemistry
Faculty of Science
Palacký University
Olomouc 771 46, Czech Republic
A. Bakandritsos
Nanotechnology Centre
Centre of Energy and Environmental Technologies
VSB – Technical University of Ostrava
17. listopadu 2172/15 708 00, Ostrava-Poruba, Czech Republic
M. Otyepka
IT4Innovations
VSB – Technical University of Ostrava
17. listopadu 2172/15, Ostrava-Poruba 708 00, Czech Republic

 The ORCID identification number(s) for the author(s) of this article can be found under <https://doi.org/10.1002/smll.202207216>.

© 2023 The Authors. Small published by Wiley-VCH GmbH. This is an open access article under the terms of the Creative Commons Attribution License, which permits use, distribution and reproduction in any medium, provided the original work is properly cited.

DOI: 10.1002/smll.202207216

a target using the systematic evolution of ligands by exponential enrichment (SELEX) technique.^[7] Currently, many aptasensors rely on complicated detection methods based on nanoparticle aggregation or require target amplification.^[8,9] Electrochemical aptasensors can simplify the detection of target molecules based on a current response related to a conformational change in the aptamer, which is conjugated to a redox probe, after target molecule binding.^[10] However, their use is so far limited to gold and glassy carbon electrodes,^[11] and low-cost, printed electrodes have not yet been explored due to their nonuniform surfaces. Thus, new carbon-based transducers are highly desired.

Graphene fulfills many requirements for an effective transducer due to its high conductivity, high surface area, and low cost. However, the low chemical reactivity and hydrophobic nature of pristine graphene hampers its functionalization^[12,13] and attachment of biorecognition units,^[14,15] as well as its effective handling and integration in devices. The low density of electrochemically active defects in pristine graphene also limits its performance in electrochemical sensing,^[16] while introducing defects and functionalities via oxidation toward graphene oxide (GO) turns graphene into an insulator^[17] and often requires gold co-deposition to increase the conductivity.^[16] Reduction steps can recover part of its conductivity but at the expense of diminishing the density of chemical functionalities. Another limitation in using GO stems from the large diversity of oxygen functionalities (e.g., hydroxyl, carboxyl, ether, epoxy, and keto groups),^[18] making its reproducible, effective and selective functionalization very challenging.

The chemistry of fluorographene^[20] bypasses such shortcomings by providing a large portfolio of selectively and densely surface-functionalized conductive graphene derivatives.^[21–23] Graphene acid (GA),^[24] with its high dispersibility in aqueous media, large number of surface-exposed carboxylic groups, electrical conductivity, and biocompatibility, can be considered an ideal scaffold for the fabrication of biosensors. GA has already been used for electrochemical sensing H₂O₂,^[25] and its carboxylic groups have been employed for covalent conjugation of biomolecules, such as enzymes.^[26] Recently, it was also utilized for conjugation with an DNA probe specific for the pig mitochondrial genome to prepare a label-free electrochemical genosensor.^[27] The conjugation relied on peptide bond formation between carboxyl groups of GA and amines of the biomolecule via carbodiimide chemistry. However, conjugation of aptamers requires specific chemistry conjugation methods to avoid aptamer damage, especially approaches that do not rely on amino groups because of their abundance in biomolecules and ability to form nonspecific crosslinks.

In this respect, click chemistry represents an ideal bioconjugation method. The term was coined by the recent Nobel Prize awardee K. Barry Sharpless in 2001 to describe reactions with high yields, wide scope, and no or few byproducts.^[27] One classical click reaction is copper-catalyzed azide-alkyne cycloaddition (CuAAC), in which an azide reacts with an terminal alkyne to form a five-membered triazole ring under ambient conditions.^[28] However, the reactions conditions must be well-tuned, as its success depends on innumerable factors such as solvent, catalyst concentration, and number of active sites and the use of biomolecules requires buffer solutions and specific conditions. The use of CuAAC to construct aptasensors is still at an

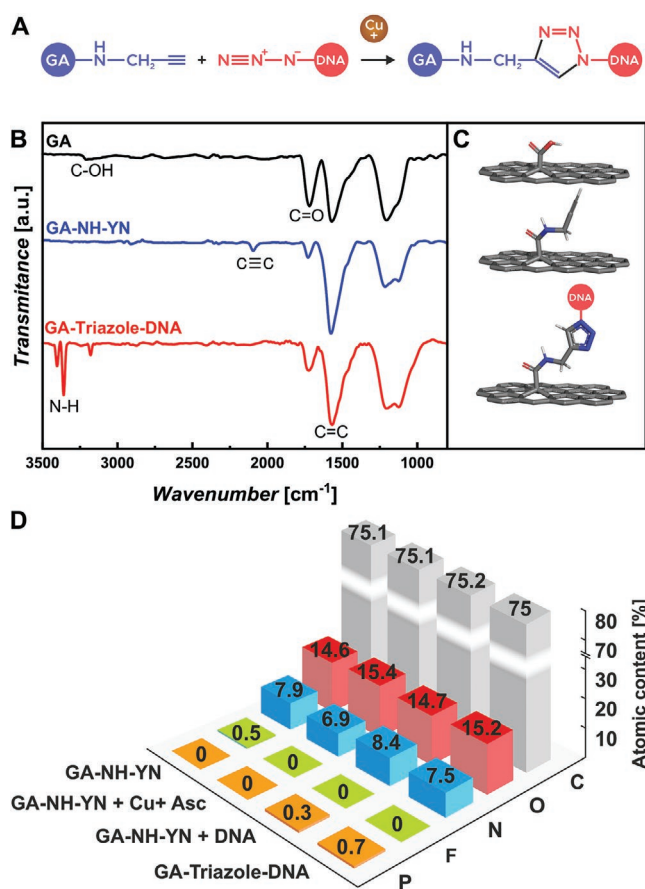


Figure 1. A) Reaction scheme depicting click chemistry between GA-NH-YN and a DNA aptamer bearing an azide moiety. B) FTIR spectra, and C) proposed structures of the starting nanomaterial (graphene acid – GA), after conjugation with propargylamine (GA-NH-YN) and click-chemistry reaction with the aptamer (GA-Triazole-DNA). D) Elemental compositions of species involved in the click-chemistry reaction by XPS analysis (see Figure S1, Supporting Information for survey XPS spectra).

early stage,^[29,30] and its potential on graphene substrates has not yet been explored.

In this work, we present a new alkyne-terminated graphene derivative (GA-NH-YN, **Figure 1**) capable of undergoing facile conjugation with biorecognition units via click chemistry. We demonstrate straightforward CuAAC conjugation with a redox-probe-modified DNA aptamer that selectively binds ampicillin. The developed electrochemical aptasensor displayed high selectivity and sensitivity to ampicillin even in complex samples, such as tap water, saliva, and milk. The developed graphene derivative provides a click-chemistry-ready system for conjugation with commercially available azide-modified biorecognition units as a versatile platform for the design of a wide portfolio of biosensors. Furthermore, GA-NH-YN allows the fabrication of flexible printed electrodes on disposable substrates for use as low-cost, point-of-interest electrochemical sensors that can be operated via a mobile phone. Importantly, these features are combined with high selectivity, even in presence of structurally similar antibiotics, and long shelf-life, while offering a detection limit for ampicillin that is eight-fold lower than the maximum residue limit for ampicillin in milk.

2. Results and Discussion

2.1. Nanomaterial Synthesis and Characterization

The carboxylic groups of GA were reacted with the primary amine units of propargylamine via carbodiimide chemistry, yielding the corresponding alkyne-terminated graphene derivative (GA-NH-YN, Figure 1). Subsequently, GA-NH-YN was conjugated via click chemistry to the DNA aptamer bearing an azide moiety after the formation of a 5-membered triazole ring (GA-Triazole-DNA) via 1,3-dipolar CuAAC.^[29]

Chemical changes during this derivatization of GA were monitored by Fourier-transform infrared (FTIR) spectroscopy (Figure 1B). The FTIR spectrum of GA-NH-YN displayed a peak at 2190 cm^{-1} , ascribed to the terminal alkyne group, confirming the successful coupling of GA with propargylamine. Moreover, the intensity of the carboxyl group band in the starting GA, centered at 1720 cm^{-1} , was significantly reduced in comparison to the other GA bands due to amide bond formation.^[24] After the click reaction of the alkyne graphene derivative with the azide-bearing aptamer, the band of the alkyne group vanished because of its conversion to a 1,2,3-triazole ring.^[32] The successful covalent conjugation of the DNA aptamer onto GA-NH-YN was indicated by the appearance of three sharp bands at 3400, 3360, and 3200 cm^{-1} attributable to N-H stretching modes of the guanine bases of the aptamer.^[33]

X-ray photoelectron spectroscopy (XPS) further proved the aptamer's successful attachment on GA-NH-YN owing to the emergence of a high atomic phosphorus content (0.7 at.%, Figure 1D, Figure S1, Table S1, Supporting Information) in the GA-Triazole-DNA product. In comparison, the product obtained by simple physical mixing of GA-NH-YN and the aptamer (without copper and the ascorbate catalyst) showed lower P content due to nonspecific sorption, verifying indirectly covalent grafting of the DNA aptamer in the GA-Triazole-DNA product.

Information about the morphology of GA-Triazole-DNA was collected by high-resolution transmission electron microscopy (HR-TEM), energy dispersive spectroscopy (EDS) elemental mapping, atomic force microscopy (AFM), and classical molecular dynamics (MD) simulations (Figure 2). A representative HR-TEM image showed that GA-Triazole-DNA consisted of very few layers of graphene (Figure 2A). EDS elemental mapping confirmed the presence and homogeneous distribution of the DNA aptamer via detection of phosphorous in the sample (Figure 2F). According to AFM measurements, the thicknesses of GA-NH-YN and GA-Triazole-DNA were 1.6 nm (or 3.1 nm for double-layer structure) and 1.9 nm, respectively (Figure S4, Supporting Information and Figure 2G). The height of GA-NH-YN derived from MD simulations was 1.7 ± 0.01 nm, corresponding well to the AFM data. MD calculations of GA-Triazole-DNA carried out in water suggested that the DNA covalently anchored to the alkyne-terminated graphene occurred in either a hairpin-like or triplex structure (Figure 2H, see also Methodology section and temperature replica-exchange MD simulations (T-REMD) discussed later for further details). The simulations indicated that the height of GA-Triazole-DNA in water reached 3.6 ± 0.2 and 4.8 ± 0.3 nm for the hairpin-like and triplex fold structures, respectively. These values are higher than those obtained by AFM, perhaps because in the AFM experiment,

sample drying caused the DNA aptamer to lose its native fold and stack more on the graphene surface.

UV-Vis spectroscopy (Figure S6, Supporting Information) also suggested DNA attachment to GA-NH-YN based on an increase in the signal at ≈ 260 nm after the click-chemistry reaction. Zeta potential measurements (Table S2, Supporting Information) revealed a higher negative potential of GA-Triazole-DNA (-20.9 mV) in comparison with bare GA-NH-YN (-10.7 mV) and the control sample obtained from simple mixing with DNA without catalyst (-13.8 mV), indicating that the negatively charged DNA aptamer was successfully attached to the nanomaterial. The Raman spectra (Figure S7, Supporting Information) show distinctive D band (at ≈ 1330 cm^{-1}) and G band (≈ 1595 cm^{-1}) bands, both reflecting the sp^2 hybridized carbon (D band with nearby sp^3 hybridized carbon, typically a defect or vacancy and G band aromatic sp^2 area).^[33,34] The I_D/I_G ratio of all three samples remained almost unchanged, with the value ranging only 1.28–1.24. However, sharp bands ≈ 2800 cm^{-1} for the GA-Triazole-DNA sample can be ascribed to the presence of the C–H vibrations coming from the aliphatic linkers of the conjugated DNA.^[35,36]

2.2. Biosensor Design and Optimization

To fine-tune the click-chemistry reaction to optimize the electrochemical response, CuAAC reaction parameters need to be studied onto the solid surface of the electrode. The ratio between copper and reducing agent and the reaction time are key parameters and thus were evaluated in this work. After 60 min of reaction, the methylene blue (MB) reduction current peak (the redox reporter on the DNA) remained constant (Figure 3A), indicating that the surface was saturated with DNA. Thus, a reaction time of 60 min was selected for further steps. The optimum ascorbate concentration was found to be 20 mM (Figure 3B); lower concentrations resulted in low reaction yields and electrochemical signal, whereas higher concentrations appeared to hinder the reaction or even damage the aptamer.^[38]

Detection of ampicillin by square wave voltammetry (SWV) was more efficient at a high frequency (100 Hz) and low amplitude (10 mV), resulting in a signal increase of 90% in comparison to that of the blank, i.e., in the absence of ampicillin (Figure 3C,D). Thus, the aptasensor exhibited “signal-on” type behavior due to the current response increase upon target binding owing to conformational changes of the aptamer and consequent approximation of the redox probe on the electrode/graphene surface. At low frequencies (25 Hz), we observed the opposite behavior, as the signal gain was negative, i.e., the response of the target was lower than in the blank, indicating a “signal-off” response. Previous studies have indicated that such behavior is dependent on the frequency applied during SWV.^[38] In our work, a frequency of 100 Hz was chosen for the next steps due to the higher signal gain.

Electrochemical experiments with the $[\text{Fe}(\text{CN})_6]^{3-/4-}$ redox probe provided valuable information about the tested materials and confirmed successful aptamer binding. Cyclic voltammetry (CV) (Figure 3E) demonstrated that the electrode modified with alkyne-graphene had significantly improved electrochemical performance since it showed higher current signals compared

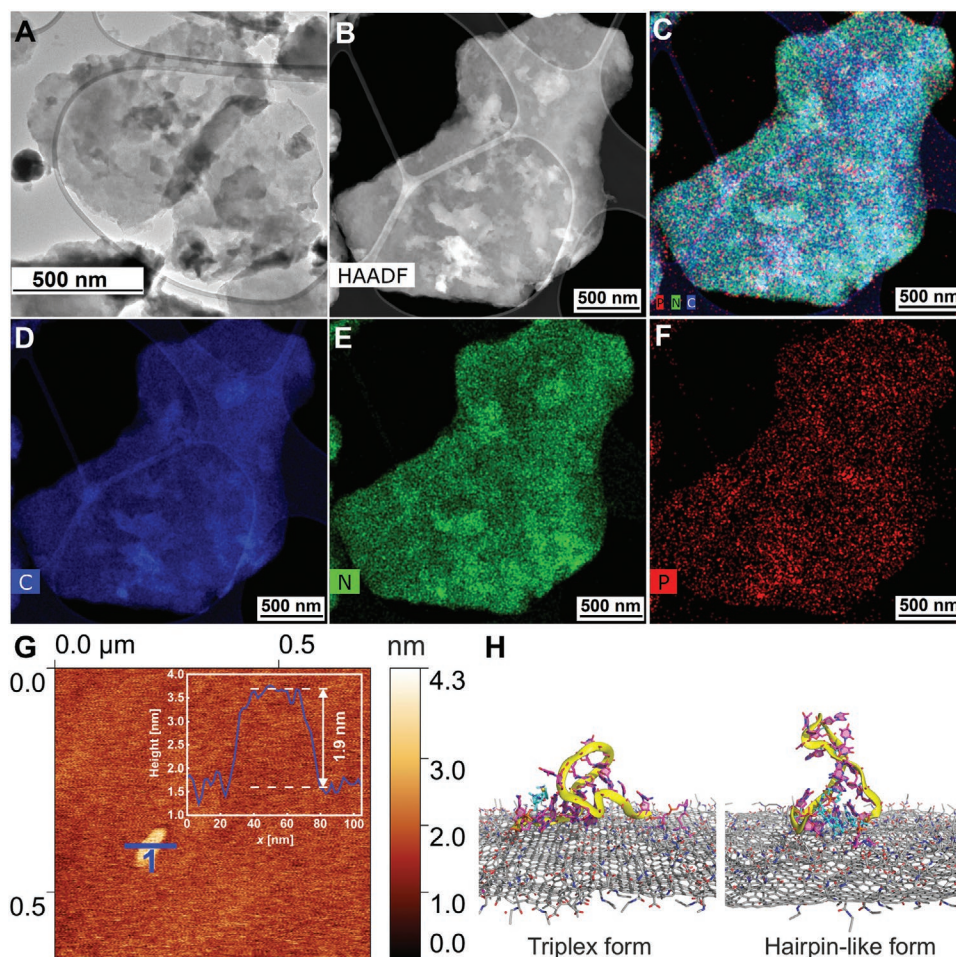


Figure 2. HR-TEM/EDS of the GA-Triazole-DNA: A) bright field, B) dark field, C) overlap of the elemental mapping of D) carbon, E) nitrogen, and F) phosphorous atoms. G) AFM analysis of GA-Triazole-DNA. H) Snapshots from free 100 ns long MD simulations showing the triplex and hairpin loop structure of the anchored DNA-aptamer on graphene acid. Both motifs showed good structural compatibility with the substrate. The methylene blue molecule (connected to the 5' end of the aptamer) is shown in cyan. Water molecules and ions are omitted for clarity.

to bare, preconditioned, and aptamer-modified electrodes. Electrochemical impedance spectroscopy (EIS) analysis and fitting with an equivalent Randles circuit (Figure 3F) revealed that the bare screen-printed carbon electrode (SPCE) was very resistive with a high charge-transfer resistance (R_{CT}) of $3620 \pm 145 \Omega$, but the acidic preconditioning improved the conductivity, lowering R_{CT} to $1640 \pm 90 \Omega$. Modification of the SPCE with the nanomaterial lowered this value further ($814 \pm 58 \Omega$), highlighting the conductive properties of the graphene derivative. After the click-chemistry reaction with the aptamer, there was an increase in R_{CT} ($1420 \pm 72 \Omega$). This may be due to the net negative charge of DNA, which repels the negatively charged $[\text{Fe}(\text{CN})_6]^{3-/4-}$ ions, combined with greater steric hindrance at the electrode surface.

2.3. Ampicillin Detection

The current response of the aptasensor varied depending on the concentration of ampicillin (Figure 4A). As the aptamer became saturated with the target, higher concentrations

showed a similar response, resulting in a logarithmic-shaped curve (Figure S8, Supporting Information) that could be linearized by applying a log function to yield the following equation $i_p = (2.2 \pm 0.1) * \log c_{AMP} + (6.8 \pm 0.6)$ ($r = 0.991$, $n = 21$), where i_p is the peak current of MB reduction (in μA) and c_{AMP} is the ampicillin concentration (in nM, see Figure 4B). The limit of detection was calculated as $3.3 * \sigma/S$, where σ is the standard deviation of the blank and S is the slope of the curve, resulting in 1.36 nM (or $\approx 0.5 \mu\text{g L}^{-1}$). This limit is higher than that of other reported biosensors for ampicillin (Table S3, Supporting Information). However, it is eight-fold lower than the European maximum residue limits in milk ($4 \mu\text{g L}^{-1}$),^[40,41] satisfying the regulatory and market needs. Moreover, the presented platform is the only one reported to date that is based on disposable carbon electrodes, offering superior cost benefits, and thus a highly competitive solution for extensive sample screening.

To evaluate the aptasensor selectivity, four other antibiotics were tested. The aptasensor has an inherent response (background current) of $10 \mu\text{A}$, which corresponds to the methylene blue reduction current in buffer solution without any binding molecule in the aptamer. The binding with the specific target

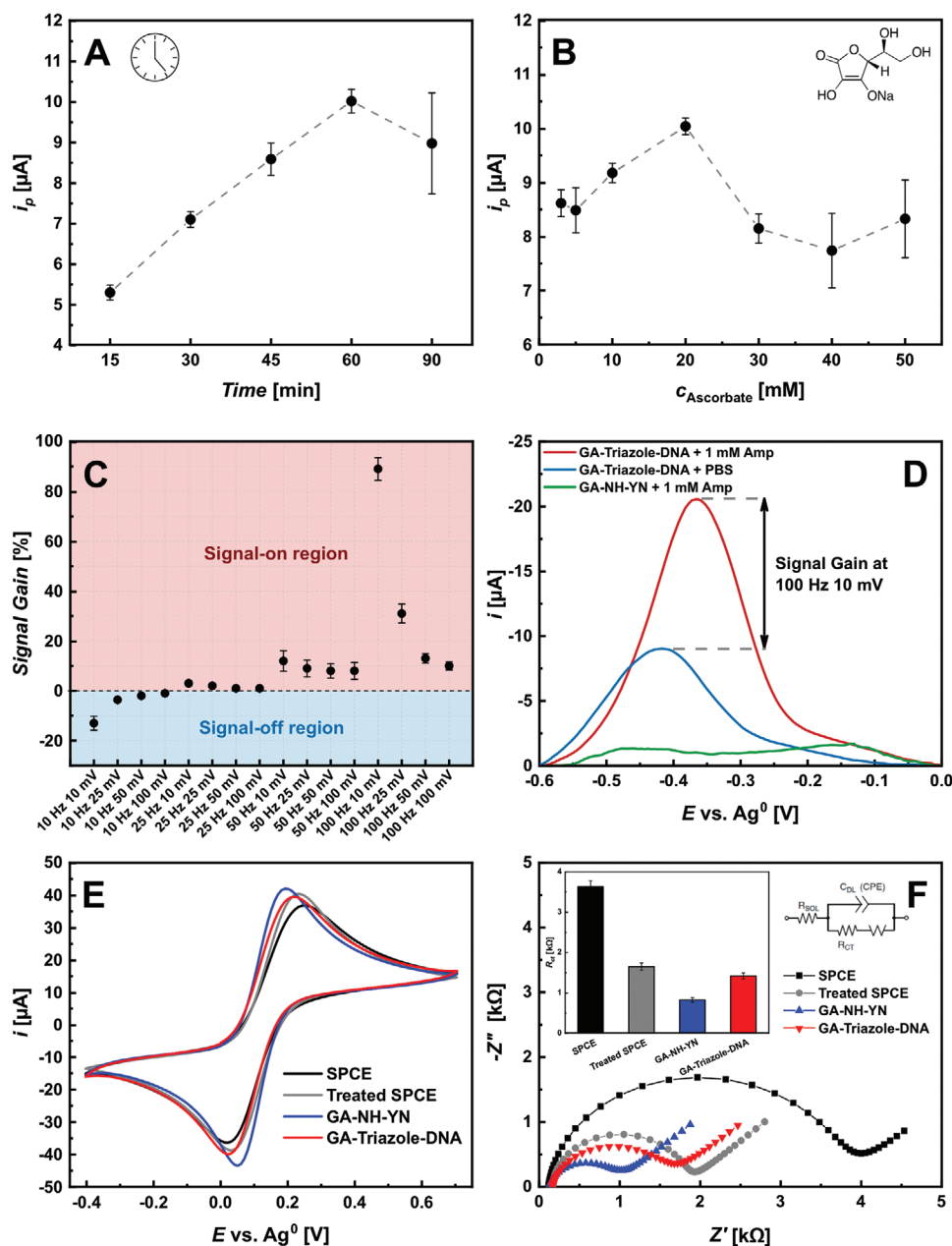


Figure 3. Click-chemistry in-situ optimization. Peak current of methylene blue reduction as a function of A) time, and B) ascorbate concentration. C) Percentage signal gain of the target and blank for different SWV parameters. D) Square wave voltammograms of methylene blue reduction with optimized parameters (100 Hz, 10 mV) with/without ampicillin and in the absence of aptamer. E) Cyclic voltammograms, and F) impedance spectra were recorded at various stages of the biosensor construction with redox probe (5 mM $[\text{Fe}(\text{CN})_6]^{3-/4-}$ in PBS solution 10 mM, pH = 7.4). All potentials are versus metallic silver.

(ampicillin) makes the current response double due to conformational changes. As the response of the aptasensor in contact with other antibiotics, including two structural analogs penicillin G and amoxicillin, was the same as the absence of target (blank), the aptasensor is highly specific (Figure 4C). The response in the presence of azithromycin and tetracycline was also equivalent to that in the blank solution (PBS-MgCl₂). After 4 weeks of storage, the aptasensor current response to ampicillin increased by 5%, probably due to changes in the conformation of the aptamer, in which the redox probe can be closer

to the electrode surface (Figure 4D). Nevertheless, this indicates excellent stability over time and demonstrates its potential as a practical and long shelf-life product.

Next, we evaluated the portable setup based on a micropotentiostat connected to a smartphone (Figure 5A) for point-of-care analysis and found that it gave only a small shift in peak potential (Figure 5B), which did not affect the sensor's performance. Further, the analysis in real samples demonstrated the ability of the aptasensor for selective detection even in complex media. The current response of the sensor in real samples

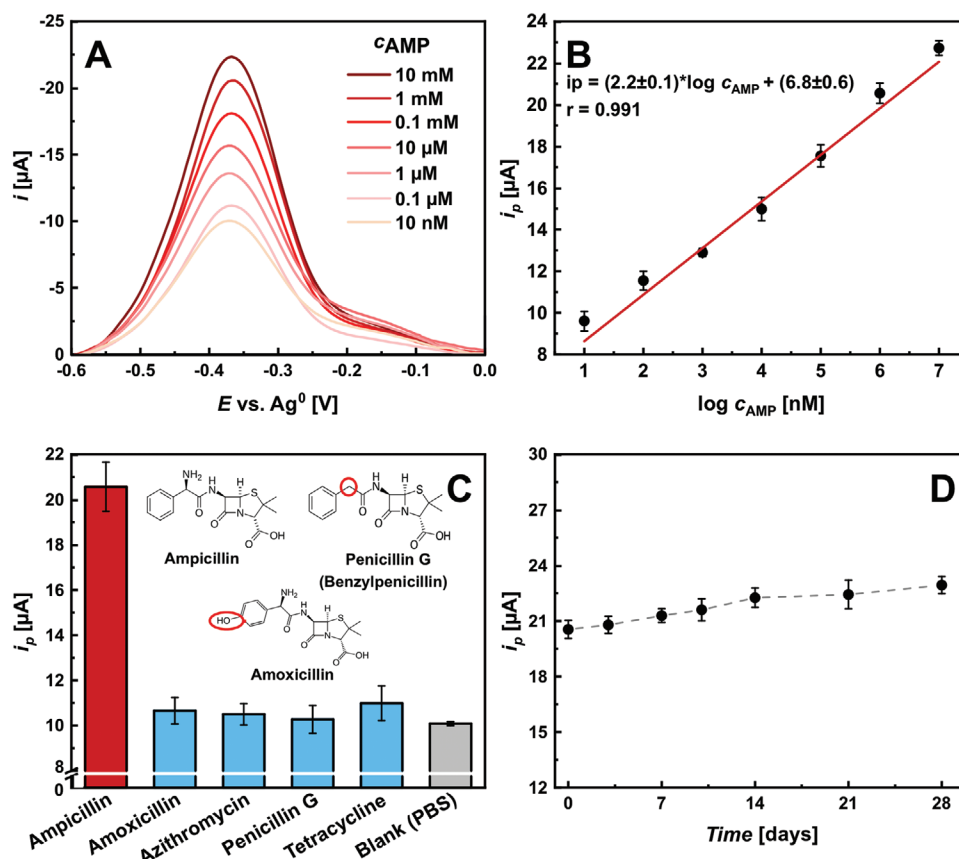


Figure 4. Ampicillin detection. A) Representative voltammograms of the response of the aptasensor in the presence of different ampicillin concentrations. B) Calibration curve of the aptasensor. C) Negative control tests, with the structures of the ampicillin analogues. D) Stability over time study. All potentials are versus metallic silver.

spiked with ampicillin was close to the signal recorded in the buffer (Figure 5C). Spiked tap water showed a recovery rate of 104%, while saliva and milk had 90% and 88% recovery rates, respectively, even though they are highly complex samples containing many potential interfering species, such as proteins, carbohydrates, and lipids (Table 1). Such superb performance and operation with the micropotentiostat connected to a smartphone opens the possibility of using the setup for real-life and affordable point-of-care analysis.

2.4. Mechanism of Action

To date, the 3D structure of the apo- and holo-forms of the ampicillin-binding DNA aptamer and the conformation of the complex remain unknown. To gain some preliminary insights into the mechanism of the ampicillin-binding DNA aptamer, we used computational chemistry tools that can describe the biomolecular systems with unprecedented temporal and spatial resolution.^[42,43] We used several sets of classical and

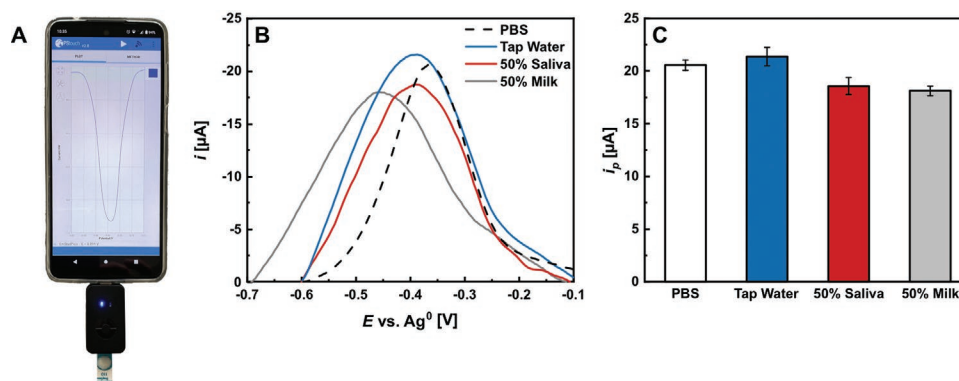


Figure 5. Real sample detection. A) Setup comprises a smartphone connected to a micropotentiostat holding a screen-printed carbon electrode. B) Voltammograms were recorded in different samples. C) Bar chart of the current response in different samples.

Table 1. The recovery rate of the aptasensor in spiked real samples.

| Sample | C _{AMP} spiked | C _{AMP} measured | Recovery rate |
|------------|-------------------------|---------------------------|---------------|
| Tap water | 1 mM | 1.040 mM | 104% |
| 50% Saliva | 1 mM | 0.904 mM | 90.4% |
| 50% Milk | 1 mM | 0.882 mM | 88.2% |

enhanced-sampling all-atom MD simulations to study the conformational behavior of DNA aptamer (see Table S4, Supporting Information for a complete list of simulations). We performed T-REMD simulations starting from the unfolded state of the DNA single-stranded aptamer in the presence or absence of ampicillin. Although the simulations were not well converged, they provided valuable insights into the structural preferences of the aptamer sequence and binding conformation of ampicillin to the DNA nucleotides. Clustering and base pairing analyses (Figure S9–11, Supporting Information) identified the locations where the system tended to form stems, and conversely, in combination with the stacking analysis, they identified positions in the sequence that were prone to bending (Figure S12–14, Supporting Information) and formation of loops. All T-REMD simulations, with or without ampicillin, showed that the aptamer had a tendency to form two loops positioned at four distinct sites in the sequence (Figures S9 and S10, Supporting Information), thereby forming a triplex-like structure.

In the T-REMD simulations with ampicillin, we focused on the behavior of the antibiotic itself, i.e., how and where it is bound. The simulations suggested that the DNA bound to ampicillin in its zero-net-charge zwitterionic form. There was almost no ampicillin-DNA binding in the T-REMD simulations of deprotonated negatively charged ampicillin (with a neutral N18 amino group). In the zwitterionic form, ampicillin bound to DNA nucleotides predominantly via the N18 ammonium group (Figure 6). This group strongly favored binding to thymine nucleotides, and showed modest binding to guanine and cytosine and no tendency to interact with adenine. In addition, we observed that the R3 phenyl ring of ampicillin tended to stack to the nucleobases. This might suggest that hydrogen

bonding of the N18 ammonium group together with stacking of the R3 phenyl ring are involved in the recognition of ampicillin by the aptamer, which would explain the selectivity of the aptamer for ampicillin over penicillin G. However, the sampling of ampicillin binding was too limited to be sufficiently predictive.

3. Conclusions

We synthesized a new conductive graphene derivative bearing alkyne groups that can undergo click-chemistry reaction with biomolecules under mild conditions. Using the classical CuAAC click reaction, we developed a simple, fast, and straightforward protocol for aptamer conjugation onto disposable, screen-printed electrodes that had been premodified with the alkyne-graphene derivative. The developed aptasensor was shown to be sensitive and selective, as demonstrated for the case of the antibiotic ampicillin. The design of the platform is versatile, as the protocol can be used with different aptamers to detect a wide variety of target analytes, thus enabling low-cost and disposable screen-printed carbon electrodes to be used for the construction of sensitive, selective, and stable point-of-care electrochemical sensors.

4. Experimental Section

Materials: All reagents were used as received without further purification. Propargylamine, anhydrous tetrahydrofuran (THF), and *N*-(3-dimethylaminopropyl)-*N'*-ethylcarbodiimide hydrochloride (EDC-HCl) were purchased from Sigma-Aldrich. Ethyl isonitrosocyanacetate (Oxyma) was purchased from Alfa Aesar. Ampicillin, amoxicillin, penicillin G, azithromycin, tetracycline, phosphate buffered saline (PBS 10 mM, pH = 7.4), potassium ferrocyanide, potassium ferricyanide, magnesium chloride, copper sulfate, sodium ascorbate, and sulfuric acid were purchased from Sigma-Aldrich/Merck. Deionized water ($\rho = 18.2 \text{ M}\Omega \text{ cm}^{-1}$) was used to prepare all solutions.

The aptamer for ampicillin was selected by Song and collaborators,^[44] which performed optical tests and chose AMP17 sequence as the best option for binding of ampicillin. It was purchased from Biomers, Germany, with modifications at both ends (Figure S2, Supporting Information)

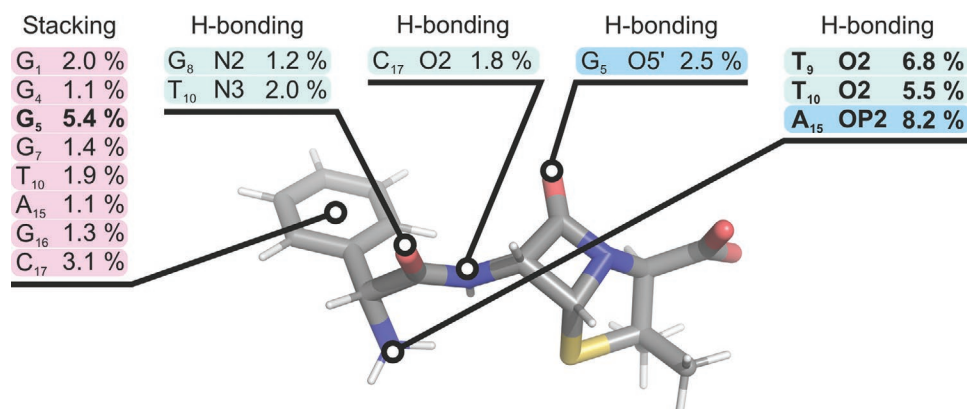


Figure 6. The population of H-bonds interactions and stacking interaction between ampicillin and DNA aptamer in the reference 298 K replica calculated from the last microsecond of T-REMD simulation of holo form (zwitterionic electrostatically neutral AMP(0)) of the d(CGGGCGTTGTATAGCGG) sequence. The blue boxes represent H-bonds between ampicillin and the backbone, green boxes between ampicillin and DNA bases, and orange boxes represent stacking interactions between phenyl ring of ampicillin and DNA bases.

as follows: 5'-(methylene blue)-GCGGGCGGTTGTATAGCGG-(azido-proline)-3'. The aptamer was resuspended in deionized water at 1 mM. For optimal binding, the aptamer was folded into its tertiary structure. Prior to use, an aliquot of 10 μL the aptamer solution was diluted to 0.1 mM in PBS containing 2 mM MgCl_2 (PBS- MgCl_2), and then heated for 5 min at 70 $^\circ\text{C}$ and cooled to room temperature (RT).

Nanomaterial Synthesis: GA was synthesized according to a previously published report.^[24] For the conjugation of GA with propargylamine to form the GA-NH-YN, a suspension of GA (30 mg) was prepared in anhydrous THF (10 mL) in a three-neck round-bottom glass flask, then EDC-HCl (444 mg, 2.32 mmol) and ethyl isonitrosocyanacetate (330 mg, 2.32 mmol) were added and the resulting mixture was stirred for 30 min at RT under a nitrogen atmosphere. Afterward, 440 μL (6.87 mmol) of propargylamine was added dropwise to the suspension and the reaction mixture was stirred for 120 h at RT. Next, the mixture was diluted in ethanol and the precipitate was collected by centrifugation. The final product was isolated by consecutive centrifugal washing steps using *N,N*-dimethylformamide, water, ethanol, and dichloromethane.

Click Chemistry in Solution: For FTIR-ATR, XPS, SEM-EDS, TEM, AFM, zeta potential measurements, and UV-vis and Raman spectroscopy analysis, the click-chemistry reaction between GA-NH-YN and the aptamer was performed in solution as follows: 700 μL of a 1 mg mL^{-1} suspension of GA-NH-YN was mixed with 100 μL of 0.1 mM azide-aptamer solution, 100 μL of 1 mM CuSO_4 solution and 100 μL of 3 mM ascorbate solution. The reaction was left to proceed for 48 h under agitation (1000 rpm) and at room temperature (25 $^\circ\text{C}$). To avoid damaging the biomolecule, sonication was not used. The nanomaterial was purified by centrifugation at 14 000 rpm for 10 min and then resuspended in 500 μL deionized water. This centrifugal washing was repeated twice more. GA-NH-YN physical mixtures with only aptamer or copper and ascorbate were used as controls.

Biosensor Construction (in situ Click Chemistry): Commercially available SPCE were used as a disposable sensing platform (DRP-110, Metrohm Drop Sens, Spain). They comprised a carbon disk working electrode (4 mm diameter), carbon auxiliary electrode, and silver pseudo-reference electrode. Before use, preconditioning was carried out in 0.1 M H_2SO_4 solution by CV (-1.5 – $+1.5$ V, 5 cycles, 100 mV s^{-1}) to remove organic crosslinks from the carbon ink, increasing the SPCE functionality and reproducibility. An Autolab potentiostat (model PGSTAT128N) was used for all electrochemical analyses unless otherwise specified.

The alkyne-graphene was deposited onto the working electrode by drop-casting according to a previously established strategy,^[27] in which the nanomaterial suspension was centrifuged for 10 min at 10 000 rpm and 20 μL of the supernatant was deposited onto the working electrode surface. After drying at room temperature, the CuAAC reaction was performed in situ at room temperature (25 $^\circ\text{C}$). A 100 μM solution of the aptamer was mixed with 1 mM CuSO_4 and various concentrations of sodium ascorbate solution in a 2:1:1 proportion, respectively. Different sodium ascorbate concentrations (3, 5, 10, 20, 30, 40, and 50 mM) and reaction times (15, 30, 45, 60, and 90 min) were tested to optimize the reaction. Afterward, the electrode surface was washed with PBS- MgCl_2 . Immobilized aptamer was detected by monitoring the reduction peak of MB by SWV using different frequencies (10, 25, 50, and 100 Hz) and amplitudes (10, 25, 50, and 100 mV) in PBS- MgCl_2 . All measurements were made in triplicate and presented as mean \pm standard deviation.

Electrochemical studies of the biosensor construction steps were performed using 5 mM $[\text{Fe}(\text{CN})_6]^{3-/4-}$ redox probe in PBS solution (10 mM, pH = 7.4). CV was measured between -0.4 V and $+0.7$ V at scan rate of 50 mV s^{-1} , EIS was measured at $E_{1/2} = 0.115$ V with a frequency range of 0.1 Hz to 10 kHz and amplitude of 10 mV.

Sample Detection: PBS- MgCl_2 containing different ampicillin concentrations (10, 1, 100, 10, 1, 100, and 10 nM) was added dropwise to the surface of the modified working electrode and left to incubate for 30 min. SWV was performed to observe the MB peak (potential range: 0–0.6 V, frequency: 100 Hz, amplitude: 10 mV). Solutions of PBS- MgCl_2 containing different antibiotics (amoxicillin, penicillin G, azithromycin, tetracycline) at 1 mM concentration were used as negative controls. The stability of the aptamer over time was evaluated by keeping the different

prepared electrodes at 4 $^\circ\text{C}$ and measuring the response in a solution of 1 mM ampicillin in PBS- MgCl_2 in a period of 4 weeks.

For test real sample detection, tap water, 50% diluted freshly collected saliva, and 50% diluted milk (1.5% fat) spiked with 1 mM ampicillin were used and the recovery percentage was calculated. A setup consisting of a micropotentiostat (Sensit Smart, Palm Sens) connected to a smartphone was utilized.

The baseline of all square wave voltammograms was subtracted and the peak current was calculated using NOVA 2.1 and PSTrace 5.9 software. To aid the presentation, the voltammograms were inverted and the most representative example was presented. Origin 2018 software was utilized to plot all data.

Simulation Setup: The unfolded starting structure of the DNA aptamer used in REMD folding and classical graphene-grafted simulations with sequence d(GCGGGCGGTTGTATAGCGG) was prepared using the Nucleic Acid Builder tool in AMBER.^[44] Additionally, for the graphene-grafted model, the secondary structure of the aptamer was predicted using the Mfold server,^[45] converted into a 3D structure using the RNAComposer server,^[46] and anchored in the middle of the graphitic surface. GA (functionalization degree 13%, of which 60% was additionally conjugated with the amino alkyne, and the remaining unmodified carboxylic groups were simulated in their deprotonated form) was modeled as a periodic sheet in the xy plane with dimensions $\approx 99 \times 101$ \AA , and unfunctionalized graphitic carbons were treated as uncharged Lennard-Jones spheres. The parameters for ampicillin in different protonation states, MB and azido-proline (N_3 -Pro) were adopted from the GAFF force-field. Partial charges for the alkyne-terminated GA (modeled on a small, functionalized pyrene model), N_3 -Pro linkers, MB and antibiotics were assessed using the RESP method at the HF/6-31G* level of theory^[47] using the Gaussian 16 program.^[48] For each set of simulations (see Table SX1, Supporting Information), all relevant molecules were subsequently assembled into a single system and the AMBER18^[49] or GROMACS 5.0 (in the case of a system with periodic graphene)^[50] packages were used to generate the starting topology and coordinates and run simulations. T-REMD^[51] and classical MD simulations of the aptamer were performed with the AMBER DNA force-field OL21^[52] including the parmbsc0^[53–55] force field with χ_{OL4} ^[56] + $\epsilon\zeta_{\text{OL1}}$ ^[57] + β_{OL1} ^[58] + α/γ ^[52] modifications. The simulations were performed by combining the SPC/E^[59] explicit water model and ~ 10 mM KCl salt excess using Joung-Cheatham ion parameters.^[60] Prior to the simulations, the prepared systems were minimized and equilibrated using the standard equilibration protocol described in the Supporting Information. The final production run for the aptamer-graphene system was carried out in the NVT ensemble for 100 ns. T-REMD simulations were run using 64 replicas at temperatures ranging from 278 to 461 K. The 64 different conformations were chosen as starting structures to ensure better convergence. The simulation time of the T-REMD simulations was at least 4 μs (Table S4, Supporting Information).

Supporting Information

Supporting Information is available from the Wiley Online Library or from the author.

Acknowledgements

The authors gratefully acknowledged support from the Technology Agency of the Czech Republic, Program TREND (GEFSEM, FW01010183), and the ERDF/ESF project “Nano4Future” (No. CZ.02.1.01/0.0/0.0/16_019/0000754). The authors acknowledged the assistance provided by the Research Infrastructure NanoEnviCz, supported by the Ministry of Education, Youth and Sports of the Czech Republic under Project No. LM2018124. This work was supported by the Ministry of Education, Youth and Sports of the Czech Republic through the e-INFRA CZ (ID: 90140). This project has received funding from the European

Union's Horizon Europe research and innovation program under grant agreement No 101059266. MO gratefully acknowledged an ERC consolidator grant (683024) from Horizon 2020. AB acknowledges funding from the Czech Science Foundation (project No 19–27454X). The authors thank Jiří Hošek, Ondřej Tomanec, and Klára Čepe for conducting the SEM, AFM, and CPEM measurements.

Conflict of Interest

The authors declare no conflict of interest.

Data Availability Statement

The data that support the findings of this study are available at ZENODO (<https://doi.org/10.5281/zenodo.7509720>).

Keywords

antibiotic detection, aptamers, biosensors, graphene acid, screen printed carbon electrodes

Received: November 20, 2022

Revised: December 20, 2022

Published online:

- [1] C. J. Murray, K. S. Ikuta, F. Sharara, L. Swetschinski, G. R. Aguilar, A. Gray, C. Han, C. Bisignano, P. Rao, E. Wool, S. C. Johnson, A. J. Browne, M. G. Chipeta, F. Fell, S. Hackett, G. Haines-Woodhouse, B. H. K. Hamadani, E. A. P. Kumaran, B. McManigal, R. Agarwal, S. Akech, S. Albertson, J. Amuasi, J. Andrews, A. Aravkin, E. Ashley, F. Bailey, S. Baker, B. Basnyat, A. Bekker, et al., *Lancet* **2022**, 399, 629.
- [2] J. O'Neill, Review on Antimicrobial Resistance <https://amr-review.org/> (accessed: November 2022).
- [3] E. C. Reynoso, S. Laschi, I. Palchetti, E. Torres, *Chemosensors* **2021**, 9, 232.
- [4] Z. V. Samsonova, O. S. Shchelokova, N. L. Ivanova, M. Y. Rubtsova, A. M. Egorov, *Appl. Biochem. Microbiol.* **2005**, 41, 589.
- [5] H. C. Ates, H. Mohsenin, C. Wenzel, R. T. Glatz, H. J. Wagner, R. Bruch, N. Hoefflin, S. Spassov, L. Streicher, S. Lozano-Zahonero, B. Flamm, R. Trittler, M. J. Hug, M. Köhn, J. Schmidt, S. Schumann, G. A. Urban, W. Weber, C. Dincer, *Adv. Mater.* **2022**, 34, 2104555.
- [6] Q. ul ain Zahra, S. A. H. Mohsan, F. Shahzad, M. Qamar, B. Qiu, Z. Luo, S. A. Zaidi, *Biosens. Bioelectron.* **2022**, 215, 114509.
- [7] F. Ghorbani, H. Abbaszadeh, J. E. N. Dolatabadi, L. Aghebati-Maleki, M. Yousefi, *Biosens. Bioelectron.* **2019**, 142, 111484.
- [8] Z. Yu, R. Y. Lai, *Talanta* **2018**, 176, 619.
- [9] A. Idili, C. Parolo, R. Alvarez-Diduk, A. Merkoçi, *ACS Sens.* **2021**, 6, 3093.
- [10] P. Dauphin-Ducharme, K. Yang, N. Arroyo-Currás, K. L. Ploense, Y. Zhang, J. Gerson, M. Kurnik, T. E. Kippin, M. N. Stojanovic, K. W. Plaxco, *ACS Sens.* **2019**, 4, 2832.
- [11] F. V. Oberhaus, D. Frense, D. Beckmann, *Biosensors* **2020**, 10, 45.
- [12] L. Liao, H. Peng, Z. Liu, *J. Am. Chem. Soc.* **2014**, 136, 12194.
- [13] J. Park, M. Yan, *Acc. Chem. Res.* **2013**, 46, 181.
- [14] I. Prattis, E. Hui, P. Gubeljak, G. S. Kaminski Schierle, A. Lombardo, L. G. Occhipinti, *Trends Biotechnol.* **2021**, 39, 1065.
- [15] E. Morales-Narváez, L. Baptista-Pires, A. Zamora-Gálvez, A. Merkoçi, *Adv. Mater.* **2017**, 29, 1604905.
- [16] H. Lee, T. K. Choi, Y. B. Lee, H. R. Cho, R. Ghaffari, L. Wang, H. J. Choi, T. D. Chung, N. Lu, T. Hyeon, S. H. Choi, D.-H. Kim, *Nat. Nanotechnol.* **2016**, 11, 566.
- [17] X. Li, L. Zhi, *Chem. Soc. Rev.* **2018**, 47, 3189.
- [18] A. Y. S. Eng, C. K. Chua, M. Pumera, *Nanoscale* **2015**, 7, 20256.
- [19] R. Zbořil, F. Karlický, A. B. Bourlinos, T. A. Steriotis, A. K. Stubos, V. Georgakilas, K. Šafářová, D. Jančík, C. Trapalis, M. Otyepka, *Small* **2010**, 6, 2885.
- [20] D. D. Chronopoulos, A. Bakandritsos, M. Pykal, R. Zbořil, M. Otyepka, *Appl. Mater. Today* **2017**, 9, 60.
- [21] D. Panáček, L. Zdražil, M. Langer, V. Šedajová, Z. Baďura, G. Zoppellaro, Q. Yang, E. P. Nguyen, R. Álvarez-Diduk, V. Hrubý, J. Kolařík, N. Chalmpes, A. B. Bourlinos, R. Zbořil, A. Merkoçi, A. Bakandritsos, M. Otyepka, *Small* **2022**, 18, 2201003.
- [22] D. D. Chronopoulos, M. Medved', P. Błoński, Z. Nováček, P. Jakubec, O. Tomanec, A. Bakandritsos, V. Novotná, R. Zbořil, M. Otyepka, *Chem. Commun.* **2019**, 55, 1088.
- [23] A. Bakandritsos, M. Pykal, P. Błoński, P. Jakubec, D. D. Chronopoulos, K. Poláková, V. Georgakilas, K. Čepe, O. Tomanec, V. Ranc, A. B. Bourlinos, R. Zbořil, M. Otyepka, *ACS Nano* **2017**, 11, 2982.
- [24] A. Lenarda, A. Bakandritsos, M. Bevilacqua, C. Tavagnacco, M. Melchionna, A. Naldoni, T. Steklý, M. Otyepka, R. Zbořil, P. Fornasiero, *ACS Omega* **2019**, 4, 19944.
- [25] H. Seelajaroen, A. Bakandritsos, M. Otyepka, R. Zbořil, N. S. Sariciftci, *ACS Appl. Mater. Interfaces* **2020**, 12, 250.
- [26] J. M. R. Flauzino, E. P. Nguyen, Q. Yang, G. Rosati, D. Panáček, A. G. Brito-Madurro, J. M. Madurro, A. Bakandritsos, M. Otyepka, A. Merkoçi, *Biosens. Bioelectron.* **2022**, 195, 113628.
- [27] H. C. Kolb, M. G. Finn, K. B. Sharpless, *Angew. Chem., Int. Ed.* **2001**, 40, 2004.
- [28] M. Meldal, C. W. Tornøe, *Chem. Rev.* **2008**, 108, 2952.
- [29] Y. An, T. Jin, Y. Zhu, F. Zhang, P. He, *Biosens. Bioelectron.* **2019**, 142, 111503.
- [30] Q. Liu, Q. Hu, L. Li, J. Kong, X. Zhang, *Anal. Methods* **2017**, 9, 3825.
- [31] M. Namvari, L. Du, F. J. Stadler, *RSC Adv.* **2017**, 7, 21531.
- [32] R. P. Lopes, M. P. M. Marques, R. Valero, J. Tomkinson, L. A. E. B. de Carvalho, *New J. Chem.* **2012**, 27, 273.
- [33] G. Kresse, J. Furthmüller, *Phys. Rev. B* **1996**, 54, 11169.
- [34] G. Kresse, J. Furthmüller, *Comput. Mater. Sci.* **1996**, 6, 15.
- [35] Z. Hu, X. Wang, W. Wang, Z. Zhang, H. Gao, Y. Mao, *Phys. Chem. Chem. Phys.* **2015**, 17, 22711.
- [36] L. Shi, C. Zheng, Y. Shen, Z. Chen, E. S. Silveira, L. Zhang, M. Wei, C. Liu, C. de Sena-Tomas, K. Targoff, W. Min, *Nat. Commun.* **2018**, 9, 2995.
- [37] G. R. Abel Jr., Z. A. Calabrese, J. Ayco, J. E. Hein, T. Ye, *Bioconjugate Chem.* **2016**, 27, 698.
- [38] P. Dauphin-Ducharme, K. W. Plaxco, *Anal. Chem.* **2016**, 88, 11654.
- [39] E. M. Agency, Committee for Veterinary Medicinal Products: Penicillins, https://www.ema.europa.eu/en/documents/mrl-report/penicillins-summary-report-committee-veterinary-medicinal-products_en.pdf (accessed: November 2022).
- [40] S. Sachi, J. Ferdous, M. H. Sikder, S. M. Azizul Karim Hussani, *J. Adv. Vet. Anim. Res.* **2019**, 6, 315.
- [41] J. Šponer, G. Bussi, M. Krepl, P. Banáš, S. Bottaro, R. A. Cunha, A. Gil-Ley, G. Pinamonti, S. Poblete, P. Jurečka, N. G. Walter, M. Otyepka, *Chem. Rev.* **2018**, 118, 4177.
- [42] M. Paloncýová, M. Pykal, P. Kůhrová, P. Banáš, J. Šponer, M. Otyepka, *Small* **2022**, 18, 2204408.
- [43] K. M. Song, E. Jeong, W. Jeon, M. Cho, C. Ban, *Anal. Bioanal. Chem.* **2012**, 402, 2153.
- [44] T. J. Macke, D. A. Case, *Molecular Modeling of Nucleic Acids*, American Chemical Society, Washington DC **1997**, 379.
- [45] M. Zuker, *Nucleic Acids Res.* **2003**, 31, 3406.

- [46] M. Antczak, M. Popenda, T. Zok, J. Sarzynska, T. Ratajczak, K. Tomczyk, R. W. Adamiak, M. Szachniuk, *Acta Biochim. Pol.* **2016**, *63*, 737.
- [47] C. I. Bayly, P. Cieplak, W. Cornell, P. A. Kollman, *J. Phys. Chem.* **1993**, *97*, 10269.
- [48] M. J. Frisch, G. W. Trucks, H. B. Schlegel, G. E. Scuseria, M. A. Robb, J. R. Cheeseman, G. Scalmani, V. Barone, G. A. Petersson, H. Nakatsuji, X. Li, M. Caricato, A. V. Marenich, J. Bloino, B. G. Janesko, R. Gomperts, B. Mennucci, H. P. Hratchian, J. V. Ortiz, A. F. Izmaylov, J. L. Sonnenberg, Williams, F. Ding, F. Lipparini, F. Egidi, J. Goings, B. Peng, A. Petrone, T. Henderson, D. Ranasinghe, et al., *Gaussian 16, Revision B.01*, Gaussian, Inc., Wallingford CT, **2016**.
- [49] D. A. Case, I. Y. Ben-Shalom, S. R. Brozell, D. S. Cerutti, T. E. Cheatham III, V. W. D. Cruzeiro, T. A. Darden, R. E. Duke, D. Ghoreishi, M. K. Gilson, H. Gohlke, A. W. Goetz, D. Greene, R. Harris, N. Homeyer, Y. Huang, S. Izadi, A. Kovalenko, T. Kurtzman, T. S. Lee, S. LeGrand, P. Li, C. Lin, J. Liu, T. Luchko, R. Luo, D. J. Mermelstein, K. M. Merz, Y. Miao, G. Monard, et al., *AMBER 2018*, University of California, San Francisco, **2018**.
- [50] D. Van Der Spoel, E. Lindahl, B. Hess, G. Groenhof, A. E. Mark, H. J. C. Berendsen, *J. Comput. Chem.* **2005**, *26*, 1701.
- [51] Y. Sugita, Y. Okamoto, *Chem. Phys. Lett.* **1999**, *314*, 141.
- [52] M. Zgarbová, J. Šponer, P. Jurečka, *J. Chem. Theory Comput.* **2021**, *17*, 6292.
- [53] A. Pérez, I. Marchán, D. Svozil, J. Šponer, T. E. Cheatham, C. A. Loughton, M. Orozco, *Biophys. J.* **2007**, *92*, 3817.
- [54] W. D. Cornell, P. Cieplak, C. I. Bayly, I. R. Gould, K. M. Merz, D. M. Ferguson, D. C. Spellmeyer, T. Fox, J. W. Caldwell, P. A. Kollman, *J. Am. Chem. Soc.* **1995**, *117*, 5179.
- [55] J. Wang, P. Cieplak, P. A. Kollman, *J. Comput. Chem.* **2000**, *21*, 1049.
- [56] M. Krepl, M. Zgarbová, P. Stadlbauer, M. Otyepka, P. Banáš, J. Koča, T. E. Cheatham, P. Jurečka, J. Šponer, *J. Chem. Theory Comput.* **2012**, *8*, 2506.
- [57] M. Zgarbová, F. J. Luque, J. Šponer, T. E. I. Cheatham, M. Otyepka, P. Jurečka, *J. Chem. Theory Comput.* **2013**, *9*, 2339.
- [58] M. Zgarbová, J. Šponer, M. Otyepka, T. E. I. Cheatham, R. Galindo-Murillo, P. Jurečka, *J. Chem. Theory Comput.* **2015**, *11*, 5723.
- [59] H. J. C. Berendsen, J. P. M. Postma, W. F. van Gunsteren, A. DiNola, J. R. Haak, *J. Chem. Phys.* **1984**, *81*, 3684.
- [60] I. S. Joung, T. E. I. Cheatham, *J. Phys. Chem. B* **2008**, *112*, 9020.